Synthesis of Fe_3O_4@nickel–silicate core–shell nanoparticles for His-tagged enzyme immobilizing agents

2016 Nanotechnology 27 495705

(http://iopscience.iop.org/0957-4484/27/49/495705)

IOP Publishing Nanotechnology
Nanotechnology 27 (2016) 495705 (9pp) doi:10.1088/0957-4484/27/49/495705

Synthesis of Fe_3O_4@nickel–silicate core–shell nanoparticles for His-tagged enzyme immobilizing agents

Moo-Kwang Shin[1], Byunghoon Kang[1], Nam-Kyung Yoon[2], Myeong-Hoon Kim[1], Jisun Ki[1], Seungmin Han[1], Jung-Oh Ahn[2,3,4] and Seungjoo Haam[1,4]

[1] Department of Chemical and Biomolecular Engineering, Yonsei University, Seoul 120-749, Korea
[2] Biotechnology Process Engineering Center, KRIBB, Cheongju 363-883, Korea
[3] University of Science and Technology (UST), 217 Gajeong-ro, Yuseong-gu, Daejeon 305-350, Korea

E-mail: haam@yonsei.ac.kr ahnjo@kribb.re.kr

Received 16 August 2016, revised 4 October 2016
Accepted for publication 18 October 2016
Published 10 November 2016

Abstract

Immobilizing enzymes on artificially fabricated carriers for their efficient use and easy removal from reactants has attracted enormous interest for decades. Specifically, binding platforms using inorganic nanoparticles have been widely explored because of the benefits of their large surface area, easy surface modification, and high stability in various pH and temperatures. Herein, we fabricated Fe_3O_4 encapsulated 'sea-urchin' shaped nickel–silicate nanoparticles with a facile synthetic route. The enzymes were then rapidly and easily immobilized with poly-histidine tags (His-tags) and nickel ion affinity. Porous nickel silicate covered nanoparticles achieved a high immobilization capacity (85 μg mg^{-1}) of His-tagged tobacco etch virus (TEV) protease. To investigate immobilized TEV protease enzymatic activity, we analyzed the cleaved quantity of maltose binding protein-exendin-fused immunoglobulin fusion protein, which connected with the TEV protease-specific cleavage peptide sequence. Moreover, TEV protease immobilized nanocomplexes conveniently removed and recollected from the reactant by applying an external magnetic field, maintained their enzymatic activity after reuse. Therefore, our newly developed nanoplatform for His-tagged enzyme immobilization provides advantageous features for biotechnological industries including recombinant protein processing.

S Online supplementary data available from stacks.iop.org/NANO/27/495705/mmedia

Keywords: enzyme immobilization, nickel silicate covered superparamagnetic nanoparticle, TEV protease, cleavage, His-tag

(Some figures may appear in colour only in the online journal)

1. Introduction

Advanced fusion protein technology has facilitated the mass production of desired proteins including high-purity enzymes. Typically, recombinant proteins produced with *Escherichia coli* (*E. coli*) using recombinant DNA containing desired coding sequences, are often conjugated with various fusion partners (e.g., maltose binding protein (MBP), N-utilizing substance A (NusA), glutathione S-transferase [1], and thioredoxin [2]) to enhance protein solubility and promote easy detection and purification [3–6]. *E. coli*-derived recombinant proteins are normally expressed in insoluble form, so fusion protein technology represents one strategy to improve protein expression [4, 5]. However, for appropriate use of ergonomically generated proteins, removal of the fused soluble proteins is essential to avoid transmutation of functional domains due to structural hindrance of the fusion partner [3, 7]. Tobacco etch virus (TEV) protease is

[4] Author to whom any correspondence should be addressed

considered one of the generally used enzymes for cleaving recombinant proteins because it is easy to produce and has high specificity [8, 9]. Significantly, effective removal of TEV protease and its reuse after the cleavage process are important to reduce product contamination directly related to desired protein purity and to improve processing economy [10, 11]. Enzyme immobilization techniques on adequate substrates are efficient ways to address this issue.

There are several types of immobilization methods available, including enzyme entrapment in the polydimethylsiloxane network membranes [12], cross-linking to form enzyme aggregates using penicillin G acylase [13], adsorption by simple physical and/or ionic bonding, or covalently binding on organic/inorganic supporting materials such as immobilization on acrylic resin [14] and zeolites [15], respectively. During the immobilization process, however, non-specific and/or random directional binding might cause severe decreases in immobilized enzyme activity. To overcome this limitation, site-specific-oriented bonding via affinity tags expressed recombinant enzymes [16], poly-histidine-tagged (His-tag) [17, 18], polystyrene binding peptide domain-tagged [19] or calmodulin protein domain-tagged [20] enzymes as examples, provide appropriate access points for successful enzyme-substrate reactions. Especially, His-tags, acting as a chelating agent, form chelate complexes with metal ions (i.e., cobalt, nickel copper, and zinc) that offer vacant electron orbitals to generate coordinate bonding [21–24]. Because the His-tag is relatively small, an immobilization system using them could minimize conformational and active change coming from structural hindrances [25]. Although using affinity tags might cause elution of immobilized proteins by dissociation of subunits that form multimeric enzymes, they still offer numerous enzymatic applications with proper binding conditions [17, 26, 27].

In particular, using nanoparticles to immobilize proteins is advantageous because of their relatively high surface areas that provide ample binding sites. Binding on inorganic nanoparticles, such as iron oxide [28, 29], gold [30], and silica nanoparticles [31] have been widely explored because of the benefits of high stability in various temperatures or pH, their own natural characteristics due to their nanosize (e.g., superparamagnetism), and straightforward surface modification. As a representative example, silica-encapsulated iron-oxide core–shell nanoparticles have various applications including magnetic resonance contrast agents [32], cell separation [33], protein purification [34], and enzyme immobilization [35]. One simple surface modification of silica is the formation of nickel silicate from SiO_2 in a one-pot synthesis step [36]. Traditionally, metal ion-modified surfaces have been applied to His-tagged protein purification and/or enzyme immobilization [37–39]. For efficient enzyme immobilization using the His-tag on nickel-surfaced magnetic nanoparticles, the system should (1) provide sufficiently large binding sites where His-tagged enzymes are bound, (2) maintain enzymatic activity after immobilization, and (3) have potential to recollect and reuse the magnetic nanoparticle-enzyme complex.

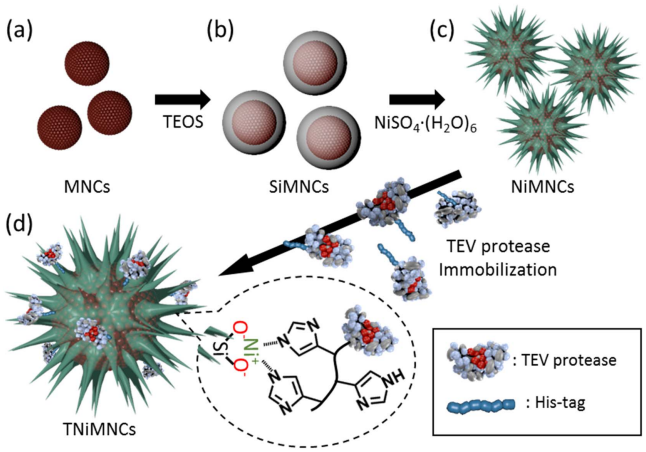

Scheme 1. Synthesis of the NiMNCs and TEV protease immobilization. ((a) Superparamagnetic iron oxide magnetic nanocluster (MNCs) was prepared by thermal decomposition method. Formation of (b) silica shell on the surface of MNCs (SiMNCs). (c) Silica shell transferred to nickel silicate (NiMNCs) and (d) His-tagged TEV protease immobilized on the surface of NiMNCs (TNiMNCs)).

Herein, we developed nickel-silicate ($NiSiO_3$)-covered magnetic nanoclusters (NiMNCs) with a silica precursor sol-gel process, followed by heat treatment with metal-ion solutions that make the shell into a porous and sea-urchin-like shape that offers effective Ni^{2+} binding sites. We then demonstrated their potential for enzyme immobilization and reusability (scheme 1). To immobilize enzymes on the Ni^{2+}-charged surface, we introduced the hexa-histidine-tagged TEV protease, and the tag simply forms chelates with NiMNCs. His-tagged TEV protease-immobilized NiMNCs (TNiMNCs) were used as the cleavage agents for recombinant proteins (maltose binding protein-exendin-fused Immunoglobulin, MBP-Ex/IgG) linked by the TEV protease specific cleavage peptide. Enzymatic activity of the immobilized TEV protease was measured by calculating the cleaved amount of MBP-Ex/IgG. After the reaction, TNiMNCs were easily recollected from the reactant using a superparamagnetic core (Fe_3O_4) with an external magnetic field. In brief, we successfully immobilized the His-tagged TEV protease on Ni^{2+}-surfaced magnetic nanoparticles, maintaining their enzymatic activity to cleave a TEV protease-specific cleaving site, ENLYFQ, inside of recombinant proteins.

2. Experiment

2.1. Materials

Sodium citrate, sodium acetate, iron (III) chloride, ethylene glycol, diethylene glycol, tetraethyl orthosilicate (TEOS), nickel (II) sulfate hexahydrate, cetyl trimethylammonium bromide (CTAB), and sodium hydroxide (NaOH) were purchased from Sigma-Aldrich. Ammonia solution, anhydrous ethanol, were purchased from Duksan. DNA plasmids of His-TEV protease and MBP-Ex/IgG were from DNA 2.0. All

chemical agents were of analytical grade and used directly without further purification.

2.2. Preparation of Fe_3O_4 nanoclusters (MNCs)

Magnetic nanoclusters were prepared with a modified solvothermal reaction. Specifically, 648 mg of $FeCl_3$, 400 mg of sodium citrate, and 4 g of sodium acetate were dissolved in 60 ml cosolvent (diethylene glycol:ethylene glycol = 2:1). The resulting mixture was then sealed in a Teflon stainless steel autoclave at 220 °C for 12 h. After cooling to room temperature, the resulting MNCs were washed several times with ethanol and deionized water and dispersed in ethanol.

2.3. Preparation of Fe_3O_4@Silica core–shell nanoparticles (SiMNCs)

SiMNCs were prepared through a sol-gel approach. Briefly, 100 mg MNCs were dispersed in 100 ml cosolvent (ethanol: deionized water = 5:1) with 4 ml ammonia solution. Next, 700 μl TEOS was added using a Harvard pump at 40 °C for 2 h with stirring. After the reaction completed, the resulting SiMNCs were washed several times with ethanol and deionized water, and dispersed in deionized water.

2.4. Preparation of Fe_3O_4@Nickel silicate core–shell nanoparticles (NiMNCs)

Nickel silicate shells were formed using silica shells as a precursor. Briefly, 50 mg SiMNCs and 196 mg nickel (II) sulfate hexahydrate were homogeneously dispersed in 20 ml deionized water. The mixture was then transferred to a Teflon stainless steel autoclave and heated to a temperature of 180 °C for 18 h. After cooling to room temperature, the resulting NiMNCs silicate core–shell nanoparticles were washed several times with ethanol and deionized water, and dispersed in phosphate-buffered saline (PBS) solution for further immobilization of His-tagged enzyme experiments.

2.5. Preparation of His-tagged TEV protease and MBP-Ex/IgG recombinant protein

Six times His-tagged TEV protease (S219V) and human IgG Fc domain fused to exendin (Ex-4), a peptide secreted from the salivary glands of the Gila monster lizard *(Heloderma suspectum*), were codon-optimized according to *E. coli* codon usage and synthesized from DNA 2.O Inc. These synthesized genes were connected to MBP by a TEV protease cleavage site, and the fusion genes were inserted into pET-30(a) (Novagen) (online supplementary figure S1). For the human IgG Fc domain fused to Ex-4 (Ex-4/IgG fc), the T7 promoter in pET-30(a) was replaced by the rhamnose promoter (figure S1). These resultant expression vectors were transformed into *E. coli* BL21 (DE3)-competent cells, respectively. The transformed *E. coli* colony was incubated at 37 °C until the optical density at 600 nm reached 0.4–0.6. Next, 0.5 mM isopropyl β-D-1-thiogalactopyranoside (IPTG) or 20 mM rhamnose was added and further incubated at 25 °C for 16 h. The BL21 (DE3) were recollected and disrupted using ultrasonication. The cell lysate centrifugation was followed by a purification step using MBP and His affinity chromatography.

2.6. Binding capacity of His-tagged TEV protease immobilized onto the NiMNC surface (TNiMNCs)

NiMNCs (1 mg) were dispersed in 1 ml His-tagged TEV protease solution with a concentration from 0 to 300 μg ml^{-1}, and gently shaken at 4 °C for 5 min. After re-moving supernatant solution and washing twice with 1 ml buffer (20 mM NaP, 0.15 M NaCl) using magnetic separation, His-tagged TEV protease immobilized NiMNCs (TNiMNCs) were redispersed in 1 ml buffer. The binding capacities were analyzed with the bicinchoninic acid (BCA) protein assay.

2.7. Investigation of immobilized enzyme activity

To test enzyme activity after immobilization, the quantities of cleaved recombinant protein using enzyme immobilized onto the NiMNCs surface was proceeded. We dispersed 50 μg immobilized TEV protease in 1 ml assay buffer containing 50 μg of recombinant protein (MBP-Ex/IgG). The cleavage reactions incubated for 24 h at room temperature with gentle agitation. The products were removed at certain time intervals of 0.5, 1, 2, 4, 10, and 24 h and inactivated with addition of sodium dodecyl sulfate (SDS) loading buffer followed by incubation at 4 °C until the next analysis. The cleaved amount of MBP-Ex/IgG was analyzed by SDS polyacrylamide gel electrophoresis (SDS-PAGE).

2.8. Immobilized enzyme reusability

To determine whether immobilized enzyme activity was preserved after reuse, we repeated the MBP-Ex/IgG cleavage test five times. Previously tested TNiMNCs were collected using magnetic separation and washed twice with buffer. Afterwards, we repeated the enzyme activity test and analysis in a same manner but the products were collected after 4 h. The remaining amount of MBP-Ex/IgG by treatment of TNiMNCs was also quantified by SDS-PAGE.

2.9. Measurements and characterization

The morphology and the size of the particles were analyzed using a transmission electron microscope (JEM-2100 LAB6, JEOL Ltd) and a field emission scanning electron microscope (JEOL-6701F, JEOL Ltd). The concentration and configuration of Fe plus Ni ions in the NiMNCs were measured by using inductively coupled plasma-optical emission spectrometry (ICP-OES) analysis (Optima 8300, Perkin Elmer) and spherical aberration correction scanning transmission electron microscope (STEM) (JEM-ARM 200F, JEOL). Nitrogen adsorption isotherms were measured using the surface analyzer ASAP 2020. The specific surface area was calculated using the Brunauer–Emmett–Teller (BET) method, and the pore diameter was calculated using the Barrett–Joyner–Halenda (BJH) method applied to the nitrogen adsorption data. BCA protein quantification was analyzed using a

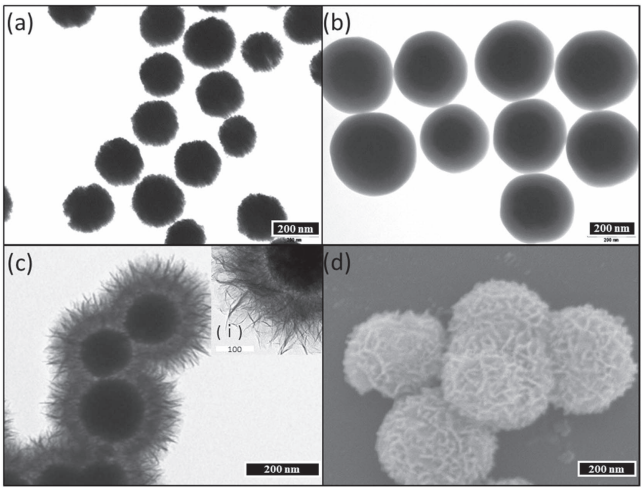

Figure 1. TEM images of (a) MNCs, (b) SiMNCs, and (c) NiMNCs; (d) SEM image of NiMNCs. The inset shows the image of NiMNCs at a higher magnification showing the porous structured shell.

microplate reader (Infinite M200 pro, TECAN). SDS-PAGE gels were captured with an ImageQuant 350 camera, and band widths were quantified with ImageJ software.

3. Results and discussion

The fabrication of spiky nickel silicate shell on the MNCs was shown in figure 1 step-by-step. Superparamagnetic MNCs with an average diameter of 190 nm were synthesized by modified solvo-thermal method [40], shown in figure 1(a). Prepared MNCs were redispersed in aqueous solution for further formation of silica shell by a modified Stöber method [41]. Monodisperse SiMNCs with 300 nm diameter and 50 nm thickness of silica shell were shown in figure 1(b). An amorphous silica shell was formed by TEOS hydrolysis under basic circumstances using NH_4OH. Because SiMNCs were used as precursors, preparation of monodispersed SiMNCs without aggregation was important. Therefore, we precisely controlled synthesis and obtained highly monodispersed SiMNCs. Figure 1(c) describes sea-urchin like shaped SiMNCs. The silica shell was transformed into a spiky nickel silicate shell, as confirmed with SEM (figure 1(d)). This nickel silicate shell has a hollow inner side volume because the silica shell was consumed to form the nickel silicate shell.

The conformational changes and the existence of nickel ions in the synthesized particles were confirmed by electron mapping by STEM and ICP-OES (figure 2). Figure 2(A) (online supplementary figure S2) shows the distributions of particle-consisting elements (Fe, O, Si, and Ni). The nickel and silicon ion spots coincided, demonstrating that the nickel silicate shell was synthesized from the silica shell. Figure 2(B) shows the ionic weight concentration. The nickel ion concentration was 149.38 μg while iron ion concentration was 539.46 μg in 1 mg of NiMNCs, indicating an overall abundance of nickel ions in the spiky shell.

Nickel silicate shell formation was also proven by Fourier transform infrared (FT-IR) spectroscopy (figure 3). MNCs represented Fe–O stretching vibration around 562 cm^{-1} over the prepared samples [42]. After formation of amorphous silica shell around MNCs, absorption peaks at 1077, 951, and 796 cm^{-1} appeared which correspond to Si–O–Si, Si–OH, and Si–O stretching vibration (figure 3(b)) [43]. However, two peaks at 951 and 796 cm^{-1} disappeared, and the peak at 1077 cm^{-1} shifted to 1005 cm^{-1} after formation of nickel silicate shell (figure 3(c)). This indicates that the Si–O–Si and Si–OH bonds disappeared upon formation of the Si–O–Ni bond [44], which implies that the amorphous silica shell was reacted as a precursor to synthesize the nickel silicate shell.

To investigate the magnetic separation property of NiMNCs, magnetic sensitivity to the external magnetic field was evaluated (figure 4). Each particle showed superparamagnetic property with no hysteresis loop; saturation magnetization value was measured to be 24.6 emu/g_{NiMNCs} (figure 4(c)). The saturation magnetization value of NiMNCs was decreased with synthesis step progressed, due to formation of nickel silicate shell over the magnetic nanoparticles so that average saturation magnetization value per equal weight of particles decreased. Undoubtedly, NiMNCs suspended in a solution were easily separated with external magnetic field and could be redispersed simply with just hand shaking after removing the magnetic field. Therefore, NiMNCs could be easily separated with external magnetic field.

XRD patterns also proved the superparamagnetism of MNCs was maintained during the synthesis step by step. The XRD pattern in figure 5(a) indicates an inverse-spinel structure of Fe_3O_4 [45]. This pattern was conserved after silica shell coating (figure 5(b)) further transformed to a nickel silicate shell (figure 5(c)), demonstrating that the crystallographic structure of core magnetic particle was not altered after formation of the nickel silicate shell, maintaining the superparamagnetism. Formation of nickel silicate shell was confirmed by the diffraction peak at 60° in figure 5(c), corresponding to (300) plane of nickel silicate [46, 47].

The surface properties of NiMNCs were measured with nitrogen adsorption isotherm using the surface analyzer ASAP 2020 to verify the large surface area and surface porosity (figure 6). Surface area was calculated by the BET method, and the pore diameter was calculated by BJH method. The BET surface area of NiMNCs was 229.8 $m^2\,g^{-1}$, significantly higher than that of MNCs and SiMNCs, 45.89 $m^2\,g^{-1}$ and 18.85 $m^2\,g^{-1}$ respectively (figure 6(A)). Simultaneously, BJH pore size of NiMNCs was 6.1 nm while that of MNCs and SiMNCs were both 1.22 nm (figure 6(B)). The surface area and pore size were effectively increased during formation of nickel silicate shell from amorphous silica. Due to the conformational change of the outer shell to become a sparse/spiky structure, NiMNCs obtained an enlarged surface area and pore size than MNCs or SiMNCs. This larger surface morphology and porosity change provided efficient TEV protease binding sites.

We next tested the binding capacity of His-tagged TEV protease, which had a molecular weight of 27 kDa, onto the NiMNC surface. As expected, the amount of immobilized His-tagged TEV protease increased with injected enzyme,

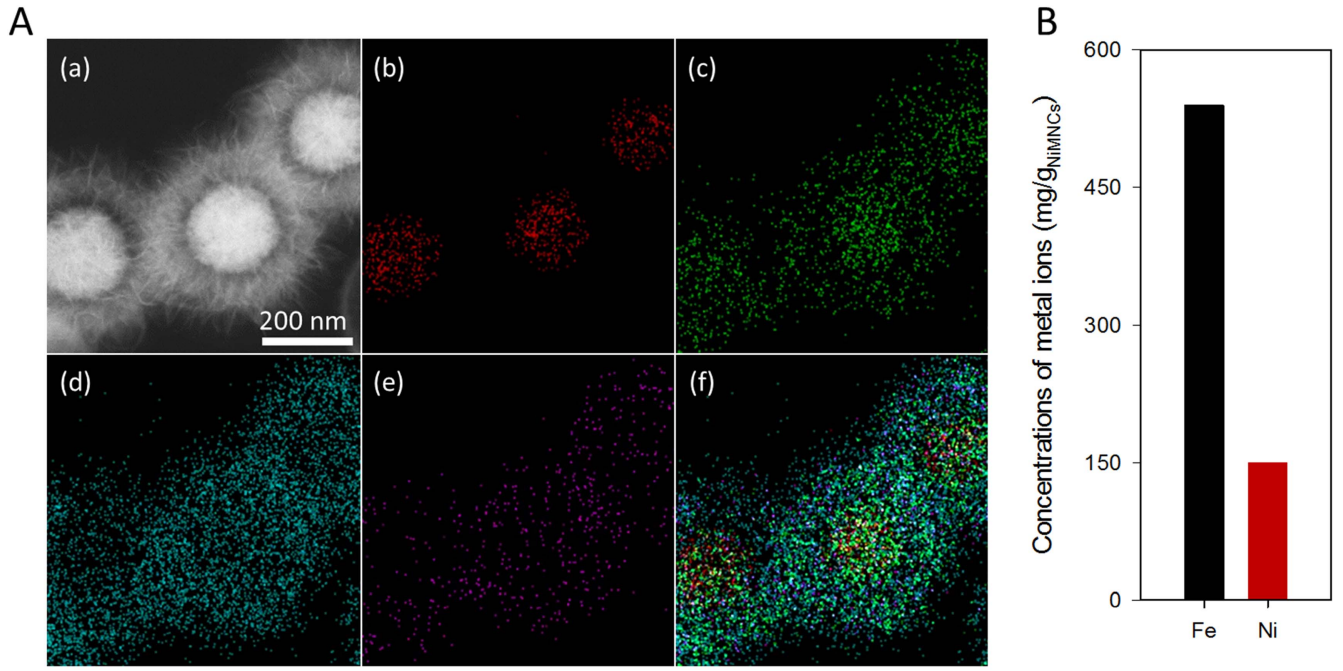

Figure 2. A: (a) STEM image of NiMNCs and (b)–(f) element mapping images of NiMNCs : (b) Fe, (c) O, (d) Si, (e) Ni, and (f) merge, B: ion concentration analyzed using ICP-OES.

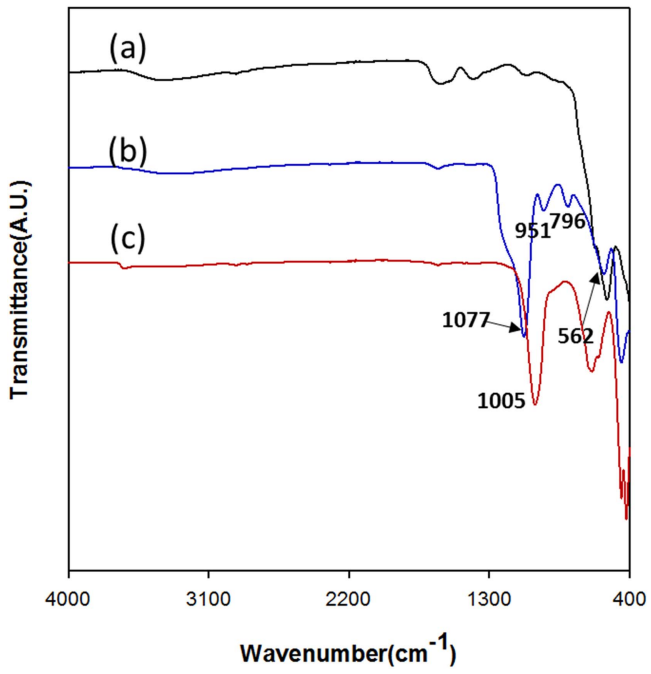

Figure 3. FT-IR spectra for (a) MNCs, (b) SiMNCs, and (c) NiMNCs.

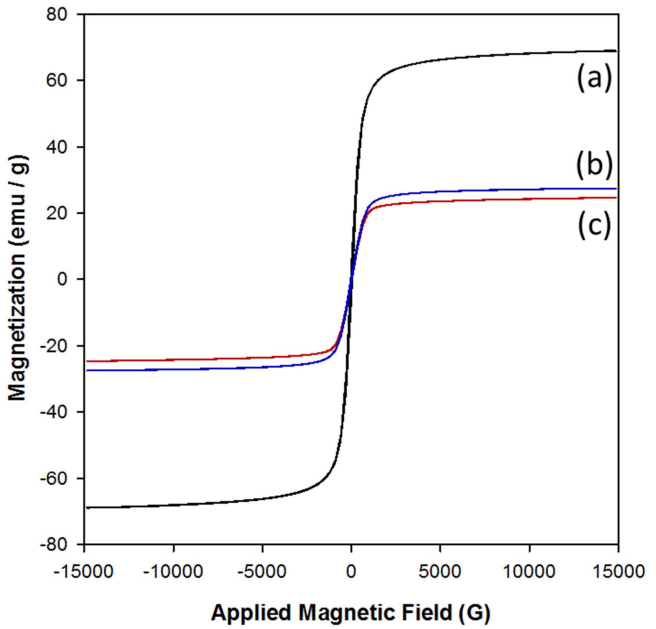

Figure 4. Magnetic hysteresis curves of (a) MNCs, (b) SiMNCs, and (c) NiMNCs.

showing a saturation curve (figure 7). The saturated amount of immobilized His-tagged TEV protease onto 1 mg NiMNCs was of the order of 85 μg. Immobilization of His-tagged TEV protease on NiMNCs was proven using FT-IR spectra to check the amide band of enzymes. -NH vibration absorption peak around 3332 cm^{-1}, and two peaks at 1642 and 1536 cm^{-1} which was corresponded to amide I (stretching vibration of the C=O bond) and amide II (bending vibrations of the N–H bond) were generated after immobilization of TEV protease on NiMNCs (online supplementary figure S3) [48, 49]. In addition, SEM images of TNiMNCs provided in online supplementary figure S4.

To confirm the effect of nickel ions for affinity binding with His-tag, binding capacity was compared with SiMNCs. The quantity of TEV protease bound on NiMNCs was 1.37-fold greater than that on SiMNCs (online supplementary figure S5). Because TEV protease (pI 9.9) become positively charged in PBS buffer (pH 7.4), they could adsorb on the surface of negatively charged NiMNCs and SiMNCs by

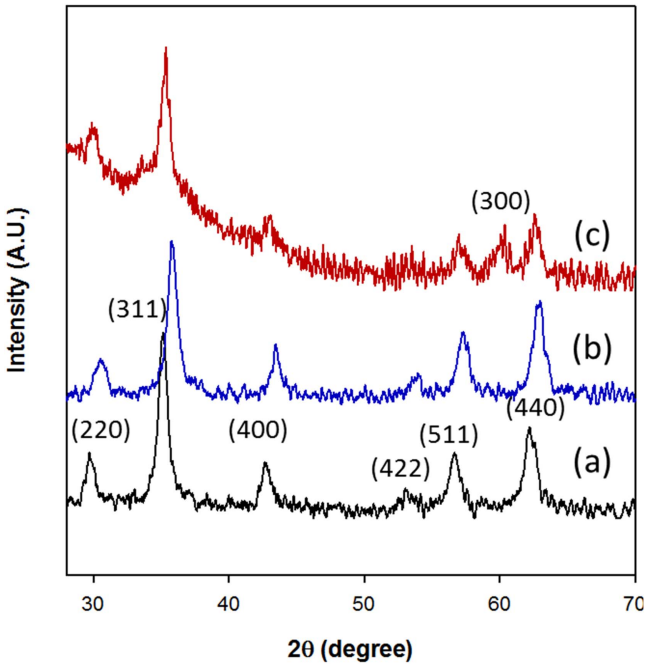

Figure 5. XRD spectra of (a) MNCs, (b) SiMNCs, and (c) NiMNCs.

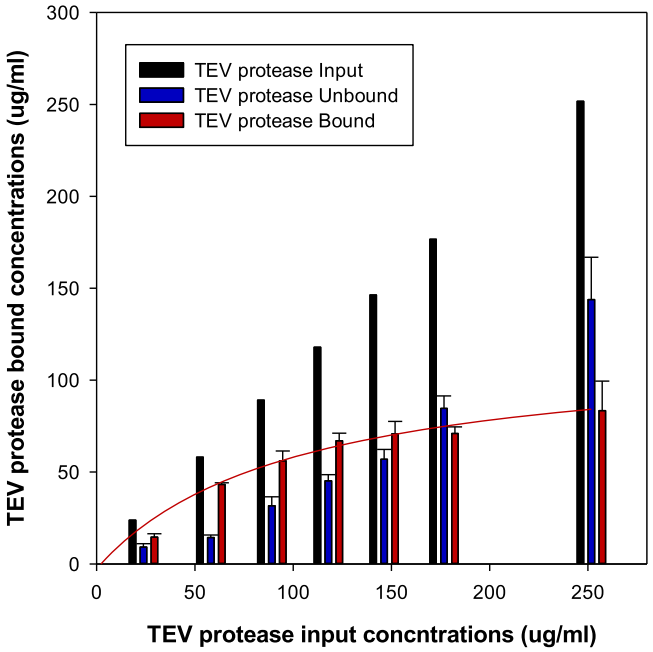

Figure 7. Enzyme immobilization capacity measurement by BCA analysis.

charge interaction [50, 51]. For a general comparison, His-tagged green fluorescent protein (GFP) was immobilized in the same way. In line with the case of TEV protease, the quantity of GFP bound on NiMNCs was 18-fold higher than that on SiMNCs (online supplementary figure S7). Both results of binding tendency were consistent in that more proteins were immobilized on the NiMNC surface with the aid of nickel ion-polyhistidine affinity. In addition, rapid enzyme immobilization occurred so that just 1 min was sufficient for fully covering the NiMNC surface with His-tagged TEV protease (online supplementary figure S8). Rapid His-tagged TEV protease binding onto the surface of NiMNCs demonstrated that well distributed nickel ions provided effective chelate-bonding sites.

To evaluate the activity of His-tagged TEV protease after immobilization on NiMNCs surface, the cleavage ratio of MBP-Ex/IgG (the recombinant protein as TEV protease substrate) was calculated at specific time intervals (0, 1, 2, 4, 6, 10, and 24 h) (scheme 2). After 4 h of agitation at room temperature, TNiMNCs cleaved 77% of MBP-Ex/IgG and

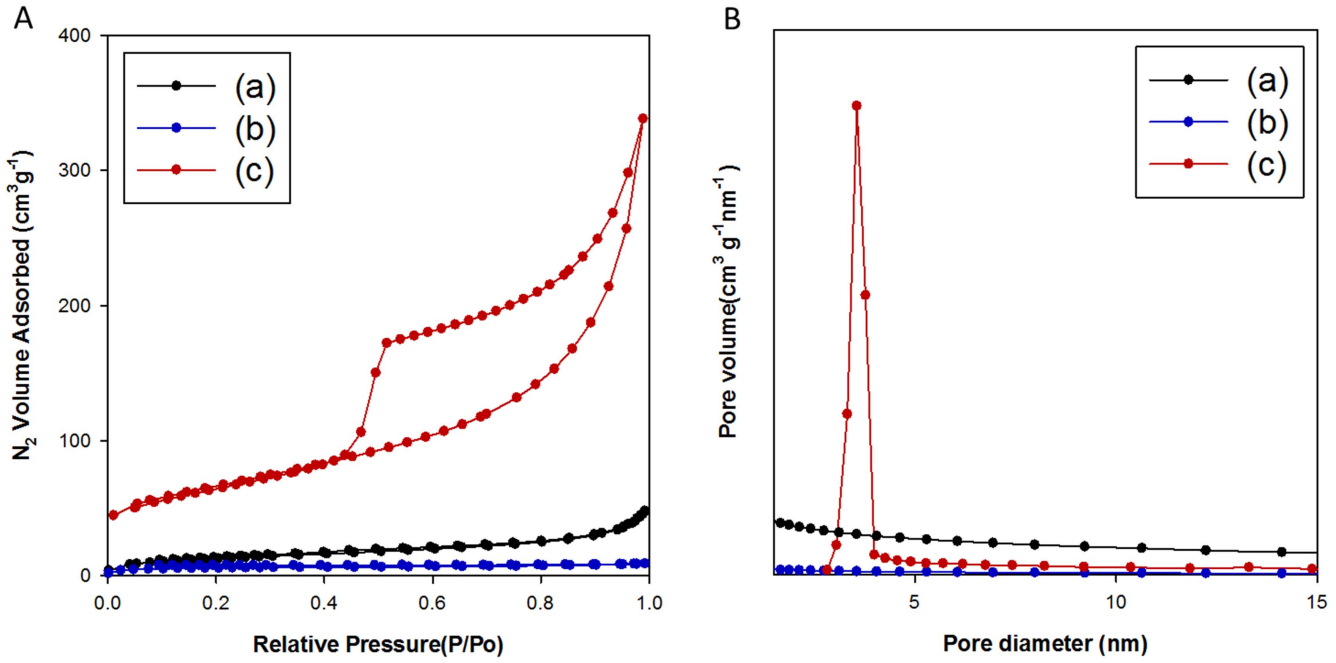

Figure 6. A: The N_2 adsorption/desorption isotherms and B: pore diameter distribution (BJH method) of (a) MNCs, (b) SiMNCs, and (c) NiMNCs.

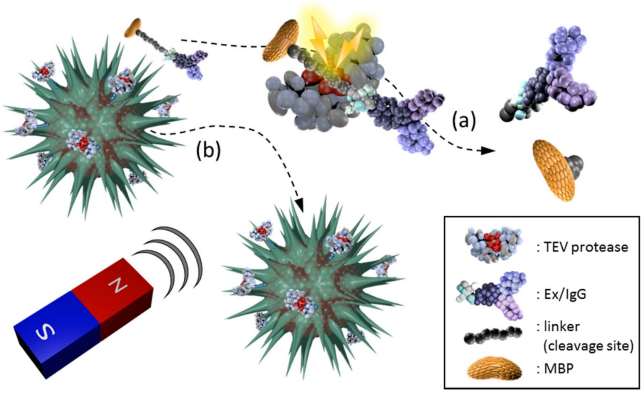

Scheme 2. Scheme for enzymatic activity of TNiMNCs cleaving of MBP-Ex/IgG. (a) MBP-Ex/IgG connected with the TEV protease specific cleavage linker, is cleaved by TNiMNCs and (b) easy-removal of TNiMNCs from reactant using magnetic field.

the cleaved amount was saturated at ~82% for the 24 h reaction. The MBP-Ex/IgG cleaved amount at 24 h reaction using TNiMNCs was 84% of that of using free His-tagged TEV protease (figure 8(a)). Fractions of cleaved MBP-Ex/IgG were run on an SDS-PAGE gel (figure 8(b)). The decreased band intensity of MBP-Ex/IgG was clearly observed, while those of MBP and Ex/IgG were increased. The results clearly show that immobilized TNiMNCs successfully maintained their enzymatic activity. On the basis of the results, specific activity was calculated for free-TEV protease and TEV protease immobilized on NiMNCs. Calculated enzyme specific activity was 32.96 $U\,mg^{-1}$ for TEV protease immobilized on NiMNCs and 47.74 $U\,mg^{-1}$ for free-TEV protease (unit activity, $U = 100$ pmol h^{-1}).

Finally, we examined the reusability of TNiMNCs to demonstrate their potential for practical industrial applications. To analyze activity maintenance, TNiMNCs were agitated with MBP-Ex/IgG for 4 h in the same way as the above activity test. For the second reaction, the activity was 73% of that of the first reaction (figure 9). From the second to fifth

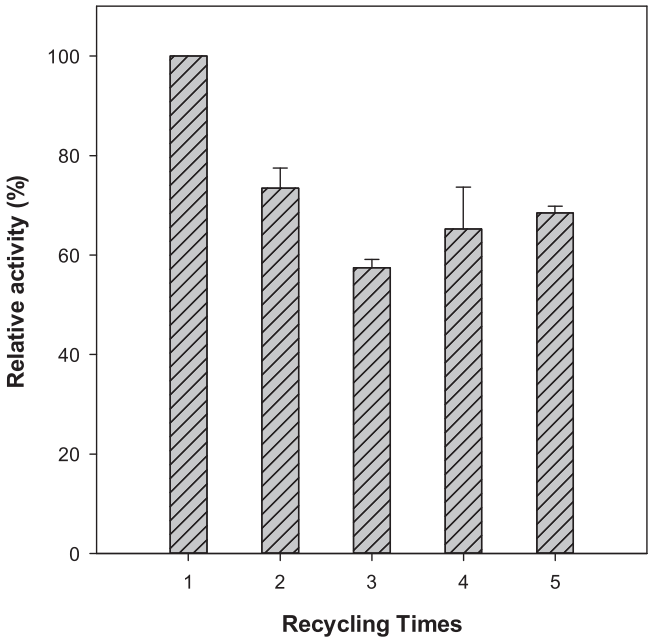

Figure 9. His-tagged TEV protease immobilized on NiMNCs in the reuse test.

recycled reaction, the activities were maintained without diminishment (figure 9). Meanwhile, TEV protease has a tendency to undergo autolysis [52]. In other words, TEV protease cleaves itself at a site similar to a specific cleaving site. As a result, one of the TEV protease immobilized the outermost side of the porous surface that was exposed to another, leading to a decrease in total enzymatic activity. However, the result was that MBP-Ex/IgG was not cleaved without TNiMNCs (online supplementary figure S9). Based on this, we can conclude that TEV protease immobilized inside of the pore and spiky surface, where another TEV protease cannot reach it. This protease was not affected by autolysis, so the real-immobilized enzymes maintained MBP-Ex/IgG cleavage activity.

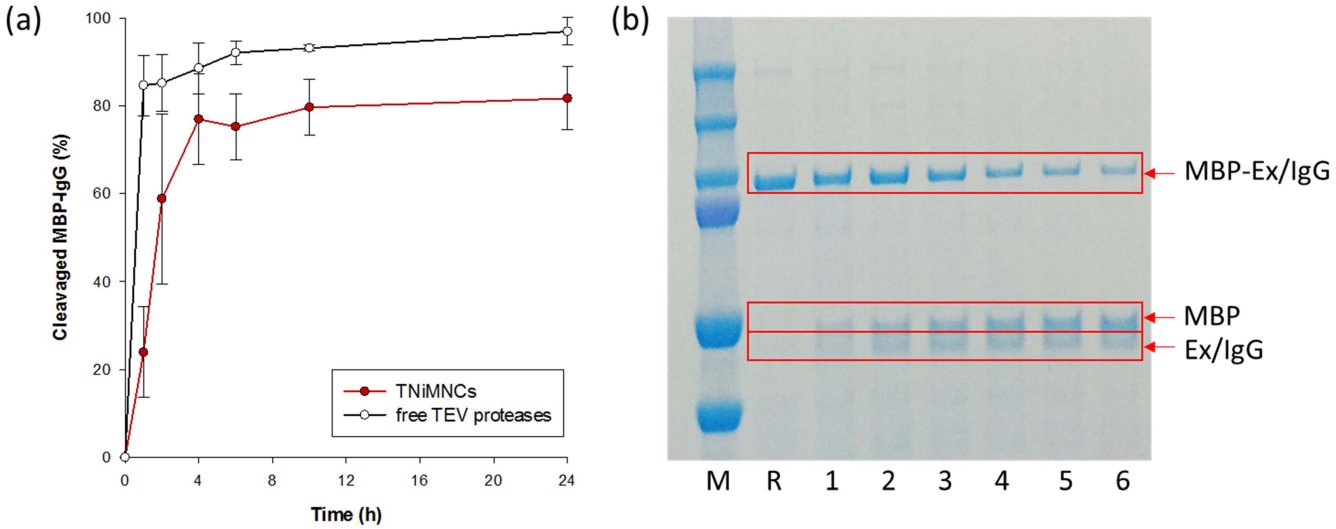

Figure 8. (a) MBP-Ex/IgG cleavage by His-TEV of free-state or immobilized on NiMNCs and (b) SDS-PAGE analysis. Lane M: molecular weight marker, lane R: initial MBP-Ex/IgG, lanes 1–6 for time intervals of 0.5-, 1-, 2-, 4-, 10-, and 24 h reaction times, respectively.

4. Conclusion

In this study, we investigated the potential use of porous nickel–silicate-covered magnetic nanoparticles (NiMNCs) as His-tagged enzyme, first report of His-TEV protease immobilized on magnetic nanoparticles. The resultant TNiMNC complexes were tested to cleave the genetically engineered recombinant protein MBP-Ex/IgG. His-TEV protease immobilization was conducted in a simple agitation process with NiMNCs, and their binding capacity was ~85 μg. Enzyme immobilization was not affected by reaction time, indicating rapid conjugation between the poly-histidine tag and nickel ion. We confirmed immobilized TEV protease activity by analyzing the cleaved quantity of MBP-Ex/IgG, and activity was preserved after recollection with a magnetic field and five reuses for five times. Our nanoplatform to His-tagged enzyme immobilization process is readily applicable for enzymatic industries such as fusion protein processes.

Acknowledgments

This research was supported by the Bio & Medical Technology Development Program of the National Research Foundation (NRF) funded by the Korean government (MEST) (NRF-2012M3A9C6050075); KRIBB Research Initiative Program.

References

[1] Smith D B and Johnson K S 1988 Single-step purification of polypeptides expressed in *Escherichia coli* as fusions with glutathione S-transferase *Gene* **67** 31–40
[2] Lavallie E R, Diblasio E A, Kovacic S, Grant K L, Schendel P F and Mccoy J M 1993 A thioredoxin gene fusion expression system that circumvents inclusion body formation in the *Escherichia coli* cytoplasm *Bio-Technology* **11** 187–93
[3] Miladi B, El Marjou A, Boeuf G, Bouallagui H, Dufour F, Di Martino P and Elm'selmi A 2012 Oriented immobilization of the tobacco etch virus protease for the cleavage of fusion proteins *J. Biotechnol.* **158** 97–103
[4] Ahuja S, Ahuja S, Chen Q J and Wahlgren M 2006 Prediction of solubility on recombinant expression of *Plasmodium falciparum* erythrocyte membrane protein I domains in *Escherichia coli Malaria J.* **5** 52
[5] Sorensen H P and Mortensen K K 2005 Soluble expression of recombinant proteins in the cytoplasm of *Escherichia coli Microbial Cell Factories* **4** 1
[6] Baneyx F 1999 Recombinant protein expression in *Escherichia coli Curr. Opin. Biotechnol.* **10** 411–21
[7] Hedhammar M, Jung H R and Hober S 2006 Enzymatic cleavage of fusion proteins using immobilised protease 3C *Protein Expres. Purif.* **47** 422–6
[8] van den Berg S, Lofdahl P A, Hard T and Berglund H 2006 Improved solubility of TEV protease by directed evolution *J. Biotechnol.* **121** 291–8
[9] Kapust R B, Tozser J, Copeland T D and Waugh D S 2002 The P1 specificity of tobacco etch virus protease *Biochem. Biophys. Res. Commun.* **294** 949–55
[10] Sheldon R A 2007 Enzyme immobilization: the quest for optimum performance *Adv. Synth. Catalysis* **349** 1289–307
[11] Cao L Q 2005 Immobilised enzymes: science or art? *Curr. Opin. Chem. Biol.* **9** 217–26
[12] Wang H Y, Kobayashi T, Saitoh H and Fujii N 1996 Porous polydimethylsiloxane membranes for enzyme immobilization *J. Appl. Polym. Sci.* **60** 2339–46
[13] Cao L, van Langen L M, van Rantwijk F and Sheldon R A 2001 Cross-linked aggregates of penicillin acylase: robust catalysts for the synthesis of beta-lactam antibiotics *J. Mol. Catalysis* B **11** 665–70
[14] Kallenberg A I, van Rantwijk F and Sheldon R A 2005 Immobilization of penicillin G acylase: the key to optimum performance *Adv. Synth. Catalysis* **347** 905–26
[15] Diaz J F and Balkus K J 1996 Enzyme immobilization in MCM-41 molecular sieve *J. Mol. Catalysis* B **2** 115–26
[16] Barbosa O, Ortiz C, Berenguer-Murcia A, Torres R, Rodrigues R C and Fernandez-Lafuente R 2015 Strategies for the one-step immobilization-purification of enzymes as industrial biocatalysts *Biotechnol. Adv.* **33** 435–56
[17] Ha E J, Kim K K, Park H S, Lee S G, Lee J O, An S S A and Paik H J 2013 One-step immobilization and purification of His-tagged enzyme using poly(2-acetamidoacrylic acid) hydrogel *Macromol. Res.* **21** 5–9
[18] Wang L A, Wei L, Chen Y A and Jiang R R 2010 Specific and reversible immobilization of NADH oxidase on functionalized carbon nanotubes *J. Biotechnol.* **150** 57–63
[19] Kumada Y, Hamasaki K, Shiritani Y, Nakagawa A, Kuroki D, Ohse T, Choi D H, Katakura Y and Kishimoto M 2009 Direct immobilization of functional single-chain variable fragment antibodies (scFvs) onto a polystyrene plate by genetic fusion of a polystyrene-binding peptide (PS-tag) *Anal. Bioanal. Chem.* **395** 759–65
[20] Daunert S, Bachas L G, Schauer-Vukasinovic V, Gregory K J, Schrift G and Deo S 2007 Calmodulin-mediated reversible immobilization of enzymes *Colloids Surf.* B **58** 20–7
[21] Kroger D, Liley M, Schiweck W, Skerra A and Vogel H 1999 Immobilization of histidine-tagged proteins on gold surfaces using chelator thioalkanes *Biosens. Bioelectron.* **14** 155–61
[22] Zachariou M and Hearn M T W 1996 Application of immobilized metal ion chelate complexes as pseudocation exchange adsorbents for protein separation *Biochemistry* **35** 202–11
[23] Porath J 1992 Immobilized metal-ion affinity-chromatography *Protein Expres. Purif.* **3** 263–81
[24] Porath J, Carlsson J, Olsson I and Belfrage G 1975 Metal chelate affinity chromatography, a new approach to protein fractionation *Nature* **258** 598–9
[25] Zhao X Y, Li G S and Liang S F 2013 Several affinity tags commonly used in chromatographic purification *J. Anal. Methods Chem.* **2013** 581093
[26] Zhao L G, Pang Q, Xie J C, Pei J J, Wang F and Fan S 2013 Enzymatic properties of *Thermoanaerobacterium thermosaccharolyticum* beta-glucosidase fused to *Clostridium cellulovorans* cellulose binding domain and its application in hydrolysis of microcrystalline cellulose *BMC Biotechnol.* **13** 101
[27] Chiang C J, Wang J Y, Chen P T and Chao Y P 2009 Enhanced levan production using chitin-binding domain fused levansucrase immobilized on chitin beads *Appl. Microbiol. Biotechnol.* **82** 445–51
[28] Verma M L, Chaudhary R, Tsuzuki T, Barrow C J and Puri M 2013 Immobilization of beta-glucosidase on a magnetic nanoparticle improves thermostability: application in cellobiose hydrolysis *Bioresour. Technol.* **135** 2–6
[29] Konwarh R, Karak N, Rai S K and Mukherjee A K 2009 Polymer-assisted iron oxide magnetic nanoparticle immobilized keratinase *Nanotechnology* **20** 225107

[30] Petkova G A, Zaruba K, Zvatora P and Kral V 2012 Gold and silver nanoparticles for biomolecule immobilization and enzymatic catalysis *Nanoscale Res. Lett.* **7** 287
[31] Soleimani M, Khani A and Najafzadeh K 2012 Alpha-amylase immobilization on the silica nanoparticles for cleaning performance towards starch soils in laundry detergents *J. Mol. Catalysis* B **74** 1–5
[32] Aptekar J W *et al* 2009 Silicon nanoparticles as hyperpolarized magnetic resonance imaging agents *ACS Nano* **3** 4003–8
[33] Kyeong S, Jeong C, Kang H, Cho H J, Park S J, Yang J K, Kim S, Kim H M, Jun B H and Lee Y S 2015 Double-layer magnetic nanoparticle-embedded silica particles for efficient bio-separation *PLoS One* **10** e0143727
[34] Aygar G, Kaya M, Ozkan N, Kocabiyik S and Volkan M 2015 Preparation of silica coated cobalt ferrite magnetic nanoparticles for the purification of histidine-tagged proteins *J. Phys. and Chem. Solids* **87** 64–71
[35] Ashtari K, Khajeh K, Fasihi J, Ashtari P, Ramazani A and Vali H 2012 Silica-encapsulated magnetic nanoparticles: enzyme immobilization and cytotoxic study *Int. J. Biol. Macromol.* **50** 1063–9
[36] Yec C C and Zeng H C 2014 Nanobubbles within a microbubble: synthesis and self-assembly of hollow manganese silicate and its metal-doped derivatives *ACS Nano* **8** 6407–16
[37] Chatterjee S, Schoepe J, Lohmer S and Schomburg D 2005 High level expression and single-step purification of hexahistidine-tagged L-2-hydroxyisocaproate dehydrogenase making use of a versatile expression vector set *Protein Expres. Purif.* **39** 137–43
[38] Ratnala V R P, Swarts H G P, VanOostrum J, Leurs R, DeGroot H J M, Bakker R A and DeGrip W J 2004 Large-scale overproduction, functional purification and ligand affinities of the His-tagged human histamine H1 receptor *Eur. J. Biochem.* **271** 2636–46
[39] Chaga G, Bochkariov D E, Jokhadze G G, Hopp J and Nelson P 1999 Natural poly-histidine affinity tag for purification of recombinant proteins on cobalt(II)-carboxymethylaspartate crosslinked agarose *J. Chromatogr.* A **864** 247–56
[40] Xuan S, Wang F, Wang Y-X J, Yu J C and Leung K C-F 2010 Facile synthesis of size-controllable monodispersed ferrite nanospheres *J. Mater. Chem.* **20** 5086–94
[41] Stöber W, Fink A and Bohn E 1968 Controlled growth of monodisperse silica spheres in the micron size range *J. Colloid Interface Sci.* **26** 62–9
[42] Wang Y, Shen Y H, Xie A J, Li S K, Wang X F and Cai Y 2010 A simple method to construct bifunctional Fe_3O_4/Au hybrid nanostructures and tune their optical properties in the near-infrared region *J. Phys. Chem.* C **114** 4297–301
[43] Sen T, Sebastianelli A and Bruce I J 2006 Mesoporous silica–magnetite nanocomposite: fabrication and applications in magnetic bioseparations *J. Am. Chem. Soc.* **128** 7130–1
[44] Wu Y H, Chang G X, Zhao Y B and Zhang Y 2014 Preparation of hollow nickel silicate nanospheres for separation of His-tagged proteins *Dalton Trans.* **43** 779–83
[45] Granitzer P, Rumpf K, Venkatesan M, Roca A G, Cabrera L, Morales M P, Poelt P and Albu M 2010 Magnetic study of Fe_3O_4 nanoparticles incorporated within mesoporous silicon *J. Electrochem. Soc.* **157** K145–51
[46] Wang Y, Wang G C, Xiao Y, Yang Y L and Tang R K 2014 Yolk-shell nanostructured Fe_3O_4@$NiSiO_3$ for selective affinity and magnetic separation of His-tagged proteins *ACS Appl. Mater. Interfaces* **6** 19092–9
[47] Liu Z, Li M, Yang X, Yin M, Ren J and Qu X 2011 The use of multifunctional magnetic mesoporous core/shell heteronanostructures in a biomolecule separation system *Biomaterials* **32** 4683–90
[48] Ding D W, Guerette P A, Hoon S, Kone K W, Cornvik T, Nilsson M, Kumar A, Lescar J and Miserez A 2014 Biomimetic production of silk-like recombinant squid sucker ring teeth proteins *Biomacromolecules* **15** 3278–89
[49] Sun P F, Hui C, Bai N L, Yang S M, Wan L, Zhang Q C and Zhao Y H 2015 Revealing the characteristics of a novel bioflocculant and its flocculation performance in *Microcystis aeruginosa* removal *Sci. Rep.* **5** 17465
[50] Blommel P G and Fox B G 2007 A combined approach to improving large-scale production of tobacco etch virus protease *Protein Expres. Purif.* **55** 53–68
[51] Nallamsetty S, Kapust R B, Tozser J, Cherry S, Tropea J E, Copeland T D and Waugh D S 2004 Efficient site-specific processing of fusion proteins by tobacco vein mottling virus protease *in vivo* and *in vitro Protein Expres. Purif.* **38** 108–15
[52] Kapust R B, Tozser J, Fox J D, Anderson D E, Cherry S, Copeland T D and Waugh D S 2001 Tobacco etch virus protease: mechanism of autolysis and rational design of stable mutants with wild-type catalytic proficiency *Protein Eng.* **14** 993–1000

Supporting Information

Synthesis of Fe_3O_4@Nickel-Silicate Core-Shell Nanoparticles for His-tagged Enzymes Immobilizing Agents

Moo-Kwang Shin[1], Byunghoon Kang[1], Nam-Kyung Yoon[2], Myeong-Hoon Kim[1], Jisun Ki[1], Seungmin Han[1], Jung-Oh Ahn[**,2,3], and Seungjoo Haam[*,1]

[1]Department of Chemical and Biomolecular Engineering, Yonsei University, Seoul 120-749, South Korea

[2]Biotechnology Process Engineering Center, KRIBB, Cheongju 363-883, South Korea

[3]University of Science and Technology (UST), 217 Gajeong-ro, Yuseong-gu, Daejeon 305-350, South Korea

E-mail: haam@yonsei.ac.kr and ahnjo@kribb.re.kr

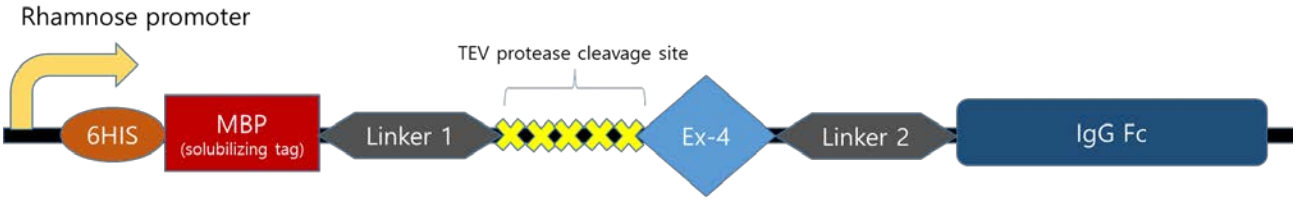

Figure S1. A schematic representation of the expression vector for the Ex-4/IgG Fc fusion protein. 6HIS, six histidine tag sequences; MBP, maltose-biding domain from E. coli; Linker1, S_3N_{10} peptide; TEV protease cleavage site, ENLYFQ; Ex-4, a peptide secreted from the salivary glands of the Gila monster lizard (*Heloderma suspectum*); Linker 2,$(G_4S)_3$ peptide; IgG Fc, human IgG1 Fc domain.

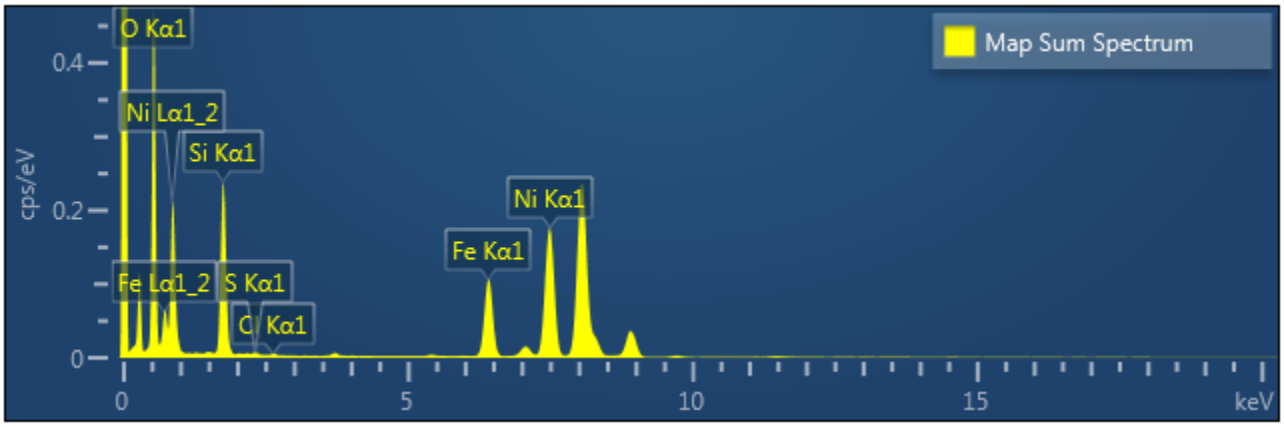

Element	Wt%	Atomic %
O	45.83	69.46
Si	17.17	14.83
Fe	13.88	6.02
Ni	22.69	9.37
Total:	100.00	100.00

Figure S2. EDS ion concentration spectrum of NiMNCs.

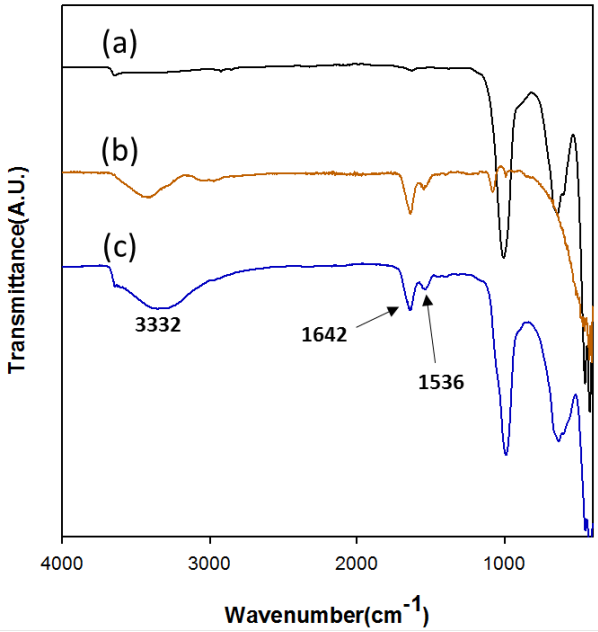

Figure S3. FT-IR spectra for (a) NiMNCs, (b) His-tagged TEV protease, and (c) TNiMNCs.

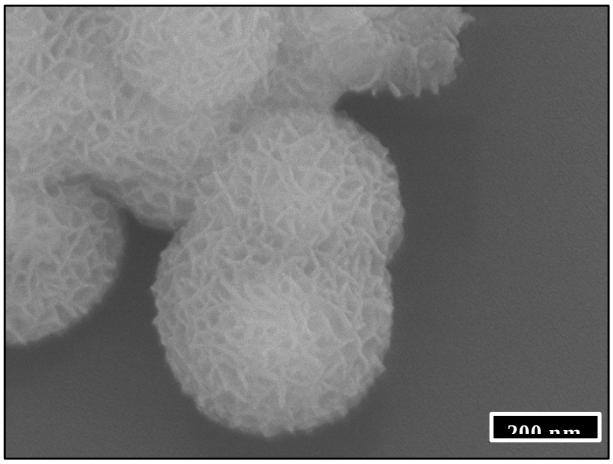

Figure S4. SEM images of TNiMNCs.

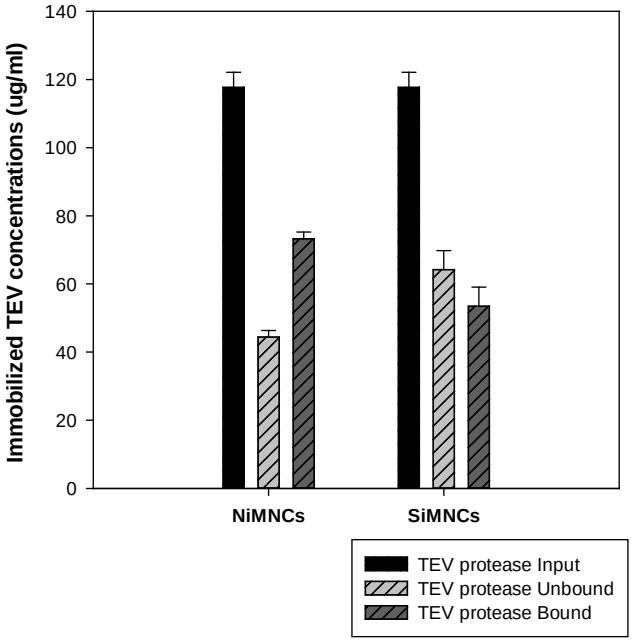

Figure S5. Comparison of TEV protease immobilization capacities between NiMNCs and SiMNCs with BCA analysis.

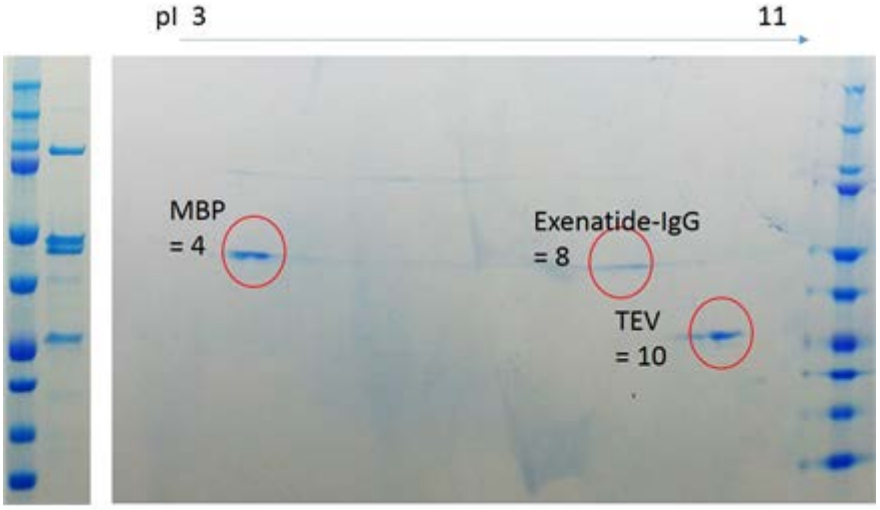

Figure S6. Isoelectric points of MBP, EX-IgG and His-tagged TEV protease analyzed using SDS-PAGE.

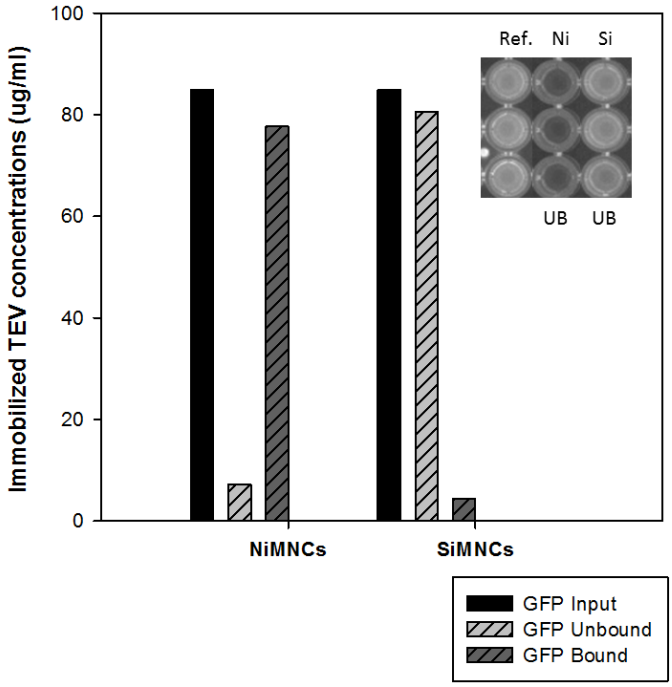

Figure S7. Comparison of GFP binding capacities between NiMNCs and SiMNCs with BCA analysis.

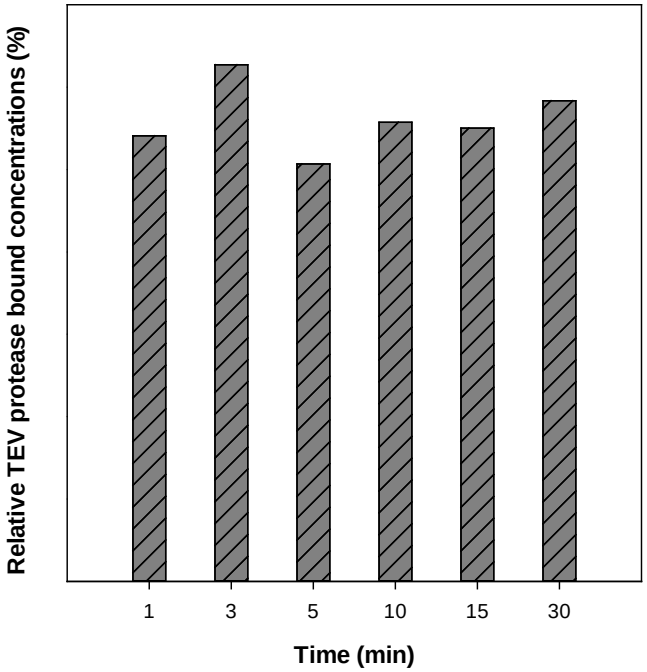

Figure S8. Comparison of TEV protease relative binding capacities on NiMNCs with different reaction times from 0 to 30 min.

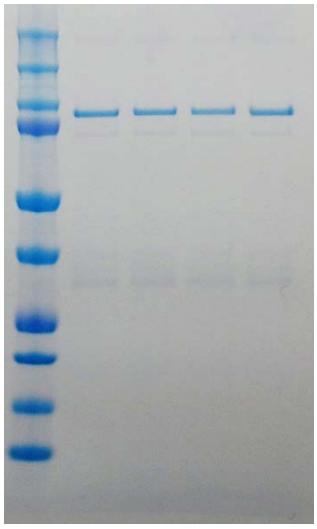

Figure S9. SDS-PAGE protein analysis of MBP-Ex/IgG shaken without immobilized TEV for 4 h.